Journal of
Water & Climate Change

IWA PUBLISHING

Journal of Water and Climate Change Vol 14 No 2, 543 doi: 10.2166/wcc.2023.384

Experimental evaluation of two-layer air bubble curtains to prevent seawater intrusion into rivers

Ehsan Kahrizi[a], Seyed Ali Akbar Salehi Neyshabouri[a,*], Amin Zeynolabedin[b], Javad Souri[a] and Hassan Akbari[a]

[a] Department of Civil and Environmental Engineering, Tarbiat Modares University, Tehran, Iran
[b] Department of Civil and Environmental Engineering, Tehran University, Tehran, Iran
*Corresponding author. E-mail: salehi@modares.ac.ir

ABSTRACT

The seawater intrusion (SWI) into rivers can lead to many negative consequences, especially on agricultural activities and live ecosystems in upstream areas of rivers. One solution to prevent SWI is using air bubble curtains (ABCs). The objective of this study is to investigate the optimal location of ABCs and airflows. To this end, several tests with different flow and salinity rates were performed and effect of ABC location on SWI investigated. The results show that, when the ratio of seawater to freshwater densities increased from 1.006 to 1.010, the ratio of saline wedge tip velocity to seawater velocity, airflow to seawater discharge ratio for first and second ABCs are raised 60, 58, and 70%, respectively. Also, when the Froude number (Fr) > 0.031, seawater density changes do not significantly affect the process of SWI. Besides, results of the study show that the closer the ABC is to the river downstream, the higher the airflow rates required. In addition, the optimal value of air bubbles for controlling SWI depends on the density of seawater, where more airflow is required to control denser flows. Finally, the regression equations to predict the SWI parameters based on flow properties were derived.

Key words: air bubble curtain, density currents, image processing method, river, salinity rate, seawater intrusion

HIGHLIGHTS

- Sustainable solution to solve seawater intrusion.
- Decreasing the negative effect of seawater intrusion on rivers.
- Feasibility to build in different sites.
- Does not have negative effect on the nature.
- It may protect freshwater resources.

GRAPHICAL ABSTRACT

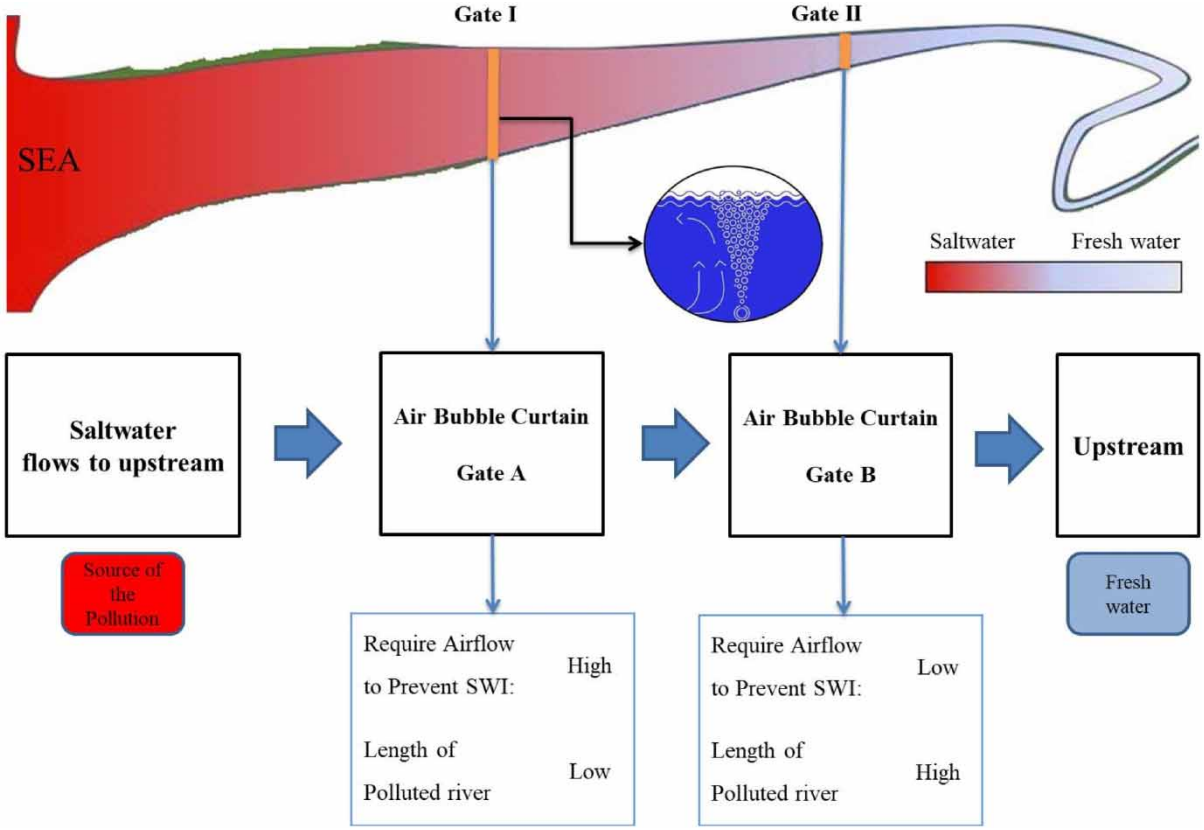

SYMBOLS AND ABBREVIATIONS

BC	Bubble column
DO	Dissolved oxygen
SCW	Sharp-crested weir
SWI	Seawater intrusion
ABC	Air bubble curtain
Q_a	Air bubble discharge
Q_s	Seawater discharge
Q_f	Freshwater discharge
LOP	Length of a river which polluted by seawater
IPM	Image processing method
ρ_s	Density of seawater
ρ_f	Density of freshwater
$V_{frontal}$	Frontal velocity of saline wedge zone
V_s	Velocity of the saline wedge at the beginning of intrusion
KH	Kelvin–Helmholtz instability
H	Hight of river's water
I_0	Intensity of struck light
I	Intensity of light transmitted from material
ε	Ability to absorb of the absorbing material
b	Length of the path in which light is absorbed
C	Concentration of the material
Reo	Reynolds number of freshwater
Fr	Froude number of freshwater
Fr_d	Densimetric Froude number

1. INTRODUCTION

Due to the population growth, the water resources are in danger of overuse and contamination (Karamouz *et al.* 2016). In coastal areas, a significant portion of the water consumption is supplied by groundwater resources (Erostate *et al.* 2020). Burgan *et al.* (2017) conducted a statistical study about extreme events in some rivers that indicated the frequency of extreme events like drought increased from 1981 to 2000 which can cause destructive results. Chebana & Ouarda (2021) studied hydrological events like floods and droughts in Iran. They developed a model that considers the non-stationary new risk assessment framework. The final model constitutes a lognormal distribution for the margins with a linear trend in the peak series, stationary for the volume series, and a quadratic trend in the logistic Gumbel copula parameter for the dependence structure (Chebana & Ouarda 2021). Overexploitation of groundwater resources, sea-level rise (SLR) due to climate changes, extreme conditions such as drought and floods lead to seawater intrusion (SWI) in coastal zones. SLR could directly affect the serviceability of infrastructures of coastal regions; effects may include intrusion of seawater into drinking water resources (Nazarnia *et al.* 2020). Soil may solute by infiltrating water, and its chemical contents affect the environment (Ekeleme *et al.* 2021). Sharp differences between fresh and seawater densities result in the formation of density currents and lead to intrusion of the tip of the seawater into the freshwater in rivers and estuaries (Zhang & Savenije 2019). SWI could damage water bodies and the neighbouring regions along rivers. Currently, more than 100 counties and locals worldwide are endangered by SWI (Barlow & Reichard 2010; Abd-Elhamid *et al.* 2016; Han & Currell 2018; Palacios *et al.* 2020; Bhagat *et al.* 2021). This issue has received more attention than ever, fostering several developments. The increasing SLR and salination of groundwater resources in coastal areas and rivers has made researchers study this phenomenon (van der Ven *et al.* 2018; Zeynolabedin *et al.* 2021a, 2021b).

It is necessary to characterize the coastal aquifer and the SWI to evaluate and mitigate the environmental risks of this phenomenon. Different approaches are applied by researchers in this regard. Zheng *et al.* (2021) studied the optimal location of cut-off walls for SWI using the Kriging surrogate model simulation and optimization model. The results show that the outputs of the Kriging surrogate model and the variable density groundwater simulation model for the same cut-off wall design fit well, and the average relative error of the two outputs is only 2.2% which proves that it is feasible to apply the Kriging surrogate model to this problem. Yusuf *et al.* (2022) provide a physical simulation to demonstrate the sand column performance of a recharge reservoir to control seawater. The results revealed a reasonably close match between physical and computational modelling. It was also found that the more sand columns and higher the reservoir water level resulted in decreased seawater penetration length. In a numerical simulation, Panpan *et al.* (2021) studied the controlling of SWI by using hydraulic and physical barriers. The results show that when the recharge well is located near the toe of the seawater wedge of 40 cm from the coastline and 5 cm from the surface, the optimal performance of the recharge scheme is achieved with a repulsion rate of up to 21.5%. When the physical barrier is located 10 cm from the coastline, and the penetration depth is 35 cm, the toe of the seawater wedge is effectively driven to the coastline with a repulsion rate of up to 81.8%. Llopis-Albert & Pulido-Velazquez (2015) used the numerical models to investigate SWI. They showed that the sharp interface approach can provide accurate results in modelling SWI when applied to transient problems. Chun *et al.* (2018) assessed the impacts of climate change and SLR on SWI in a coastal aquifer by using the Saturated-Unsaturated Transport (SUTRA) model. The results showed that the largest increase in salinity occurred (40.3%) from the scenario of 57 cm in SLR. Abd-Elhamid *et al.* (2019) evaluated the impact of reservoir dam on SWI in the Nile Delta Aquifer, Egypt using a numerical method. They concluded that the maximum groundwater drawdown will reach 2.65 m and seawater will advance significantly by constructing the new dam. Torres-Martinez *et al.* (2019) developed a geophysical model to assess SWI in a coastal aquifer in Mexico. This model was based on a density-dependent flow model to simulate groundwater flow and SWI. The results indicated that due to the high rate of pumping for agricultural use in the past decade, a large cone of depression had formed, leading to the SWI advancement on the order of 6–8 km inland in the northern-central part of the aquifer. Zeynolabedin *et al.* (2021a, 2021b) assessed the uncertainty of geoelectrical models in modelling SWI in the coastal aquifer of Chaouia, Morocco. The general results indicated that the seawater has intruded about 2 km into the shore. The uncertainty analysis showed that there was a sensible difference between the maximum and minimum extent of SWI (maximum 9% variation in the area of SWI) which should be noted when doing water research management studies.

Besides modelling SWI and assessing the current status of coastal aquifers, researchers proposed different appropriate mitigation strategies in previous studies. One of the common alternatives to solving or reducing this negative effect is to decrease the intrusion length of the saline wedge (Nakai & Arita 2002; Zeynolabedin & Ghiassi 2019). The initial solution to cutting

down the SWI length is creating a mound or a weir on the bottom of the channels, which also has side effects such as reducing the flood run-off capability of the channels. A superior alternative for narrow rivers is using air bubble curtains (ABCs). Not only is this solution easy to build but also it does not decrease the flood run-off capability (Nakai & Arita 2002). Moreover, it increases the dissolved oxygen (DO) by injecting bubbles into the water, which is notable in enhancing water quality (Larsen *et al.* 2019). Most of the studies carried out on the application of ABCs have focused on the density current in lock exchanges (Sasaki & Asaeda 1993; Asaeda *et al.* 1997; Oldeman *et al.* 2020). Nakai & Arita (2002) investigated steady saline wedge behaviour with the addition of ABC to find out more about the flow mechanism around an air curtain. Based on the findings, ABCs can significantly prevent SWI in different scenarios. Recently, Talebi & Salehi Neyshabouri (2021) studied the effect of ABCs on SWI in a numerical assessment with various seawater density rates and with river water levels as the main variable. The results showed that the ABC method is a good solution for SWI challenges. Bacot *et al.* (2022) established a formal analogy between bubble curtains and air curtains and unified the two frameworks. By means of small-scale laboratory experiments conducted in a channel with freshwater and brine solutions, they studied how effectively a bubble curtain acts as a separation barrier for a wide range of density differences as well as different air fluxes and water depths. The results showed high applicability of this approach. Talebi *et al.* (2022) investigated the effect of seawater density and air bubbles discharge on the performance of the air bubbles curtain using a numerical model. The results showed that the ABCs can prevent salinity intrusion by forming a vertical flow. Also, they concluded that there is an optimal discharge that discharges greater than it has insignificant effects on ABCs performance.

Reviewing the literature revealed that most previous studies focused on a single linear ABC, while ignoring the optimal location of ABC installation along a polluted river. This is important in terms of economic approaches because the length of the intrusion in actual conditions sometimes exceeds tens of kilometres. The cost of providing airflow in ABC in different locations vary since intrusion fluxes might decrease by moving in the upstream direction. Also, the minimum value of airflow to prevent SWI in different scenarios is another question that directly affects the feasibility of such ideas in field projects. In order to fill these gaps, this experimental study is focused on investigation of the optimal location of ABC regarding the changes in the density of seawater, velocity, and depth of the river by using two different linear ABCs. Also, this study attempts to investigate the optimal air bubble flow for controlling SWI.

2. MATERIALS AND METHODS

2.1. Experimental set-up and test cases

A 2D straight flume of 200 cm in length, 5 cm in width, and 50 cm in height was used in this experiment (Figure 1). The freshwater flowed from upstream (right side) to downstream (left side), and the depth of the river was controlled by a sharp-crested weir (SCW) installed at the end of the reservoir. Saline wedge intrusion was created in the flume by releasing seawater from the outlet installed at the end of the downstream edge to the upstream side.

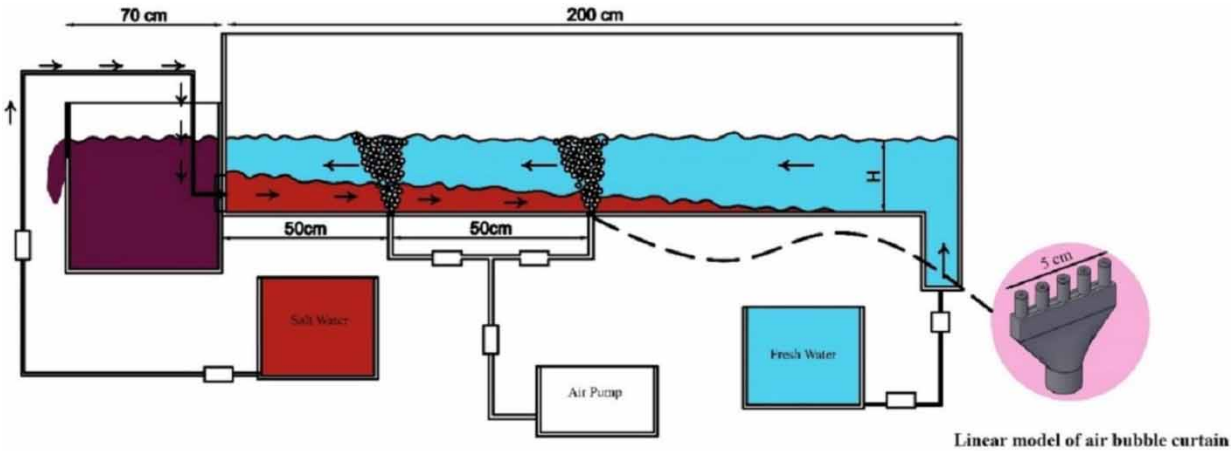

Figure 1 | Experimental set-up's side view.

Two linear air curtains were separately installed perpendicularly to the stream-wise direction at the bottom of the flume to create air. The distance from the first ABC (ABC-I) and the second ABC (ABC-II) to the downstream edge was 50 and 100 cm, respectively. The curtains had five circular holes. The distance between the holes was 1 cm with each hole 1 mm in diameter. An air compressor was used to create bubbles in the flume. A flowmeter measured the airflow rate (see Figure 1).

The experimental conditions are shown in Table 1. The variables of the study included freshwater discharge per unit width (q_f), river depth (H), and seawater density (ρ_s). Some experimental assumptions made are as follows:

- The slope of the flume is zero.
- The cross-section is rectangular.
- There is no friction between the flume and water.
- The injected air pressure is 1 atm and the water temperature is around 25 °C.

The air bubble discharge per unit of width under standard atmospheric pressure (q_a) was measured as the response parameter. Reo, Fr_d, and Fr are the channel Reynolds number, channel densiometric Froude number, and channel Froude

Table 1 | Test cases

Test case	$Q_{f\text{-}LPM}$	$Q_{s\text{-}LPM}$	H (cm)	ρ_s (g/cm^3)	Fr_d	Fr	Reo
T1	32	1.67	23	1.006	0.380	0.0309	10614
T2	32	1.67	23	1.008	0.333	0.0309	10614
T3	32	1.67	23	1.010	0.300	0.0309	10614
T4	32	1.67	24	1.006	0.356	0.0290	10614
T5	32	1.67	24	1.008	0.312	0.0290	10614
T6	32	1.67	24	1.010	0.281	0.0290	10614
T7	32	1.67	25	1.006	0.335	0.0272	10614
T8	32	1.67	25	1.008	0.294	0.0272	10614
T9	32	1.67	25	1.010	0.265	0.0272	10614
T10	34	1.67	23	1.006	0.404	0.0328	11277
T11	34	1.67	23	1.008	0.354	0.0328	11277
T12	34	1.67	23	1.010	0.319	0.0328	11277
T13	34	1.67	24	1.006	0.379	0.0308	11277
T14	34	1.67	24	1.008	0.332	0.0308	11277
T15	34	1.67	24	1.010	0.299	0.0308	11277
T16	34	1.67	25	1.006	0.356	0.0289	11277
T17	34	1.67	25	1.008	0.312	0.0289	11277
T18	34	1.67	25	1.010	0.281	0.0289	11277
T19	36	1.67	23	1.006	0.427	0.0347	11940
T20	36	1.67	23	1.008	0.374	0.0347	11940
T21	36	1.67	23	1.010	0.337	0.0347	11940
T22	36	1.67	24	1.006	0.401	0.0326	11940
T23	36	1.67	24	1.008	0.351	0.0326	11940
T24	36	1.67	24	1.010	0.316	0.0326	11940
T25	36	1.67	25	1.006	0.377	0.0307	11940
T26	36	1.67	25	1.008	0.330	0.0307	11940
T27	36	1.67	25	1.010	0.298	0.0307	11940

number, respectively, which are obtained as follows (Equations (1)–(3):

$$\mathrm{Reo} = \frac{q_f}{\nu} \tag{1}$$

$$\mathrm{Fr_d} = \frac{q_f}{(g'H^3)^{1/2}}, \quad g' = \left(\frac{\rho_s - \rho_f}{\rho_f}\right) \times g \tag{2}$$

$$\mathrm{Fr} = \frac{V}{(gH)^{1/2}} \tag{3}$$

where g', V, g, and ν denote the buoyancy acceleration, freshwater velocity, gravitational acceleration, and the kinematic viscosity, respectively.

Two-dimensional analyses were performed to investigate the flow characteristics (Equations (4) and (5):

$$\frac{Q_a}{Q_s} : f\left(\frac{\rho_s}{\rho_f}, \ \mathrm{Fr_d}\right) \tag{4}$$

$$\frac{V_{\mathrm{frontal}}}{V_s} : f\left(\frac{\rho_s}{\rho_f}, \ \mathrm{Fr}\right) \tag{5}$$

where Q_a, Q_s, V_s, and V_{frontal} denote discharge of the air bubbles, discharge of the seawater, velocity of the seawater, and tip velocity of the saline wedge, respectively.

2.2. Method

In the experiment, a steady salt wedge without any ABC was produced in the flume (Figure 2). Then, an ABC was produced by releasing bubbles from the linear ABC. ABC-I and ABC-II were placed in different locations. Once the salt wedge was steadily formed, ABC-I was opened, gradually increasing the air flow rate as all the seawater mass returned downstream by the effect of the bubble curtain (Figure 2(b)). Next, the optimal amount of the air discharge required to control the seawater was obtained for ABC-I. Also, the flow characteristics around ABC-I was observed and photographed. Then, the air flow of ABC-I was closed, after which the salt wedge gradually formed again. Subsequently, ABC-II was gradually opened and all the previous steps were repeated to find the optimal air flow discharge of ABC-II (Figure 2(c)). With this procedure, the effect of ABC location on SWI was considered. Figure 3 presents the flowchart of the research methodology.

The image processing method (IPM) was used to trace the flow concentration and distribution of SWI. IPM provides an unintrusive technique for generating high-resolution concentration data in experimental studies. Quantifying the mixing level in SWI by IPM requires establishing a link between pixel intensity and dye concentration which is provided by Beer–Lambert Law (BLL). BLL was used to determine concentration profiles in flows through porous media by Ghisalberti & Nepf (2005). Also, potassium permanganate was used as a tracer to investigate the salt concentration of seawater wedges in a flume (Figure 4).

Based on this law, when light reaches material that absorbs light, the relationship between the intensity of the impact light (I_0) and the intensity of the light transmitted from material (I) is as follows (Equation (6)) (Ghisalberti & Nepf 2005):

$$\mathrm{Log}\left(\frac{I_0}{I}\right) = \varepsilon bc \tag{6}$$

where ε is the ability to absorb light from materials, b represents the length of the path in which the light is absorbed, and C denotes the concentration of the material.

3. RESULTS

3.1. Velocity of frontal wedge

The effects of Frd, ρ_s/ρ_f, and Fr on V_{frontal}/V_s ratio are shown in Figure 5. Based on Figure 5(a), $\mathrm{Fr_d}$ number increases by almost 65%, as the V_{frontal}/V_s ratio is reduced by about 66%. Also, the line trend will be constant when the $\mathrm{Fr_d}$ number increases. The R^2 of the model for the $\mathrm{Fr_d}$ equation is 0.89, indicating that the model is significant. Figure 5(b) demonstrates

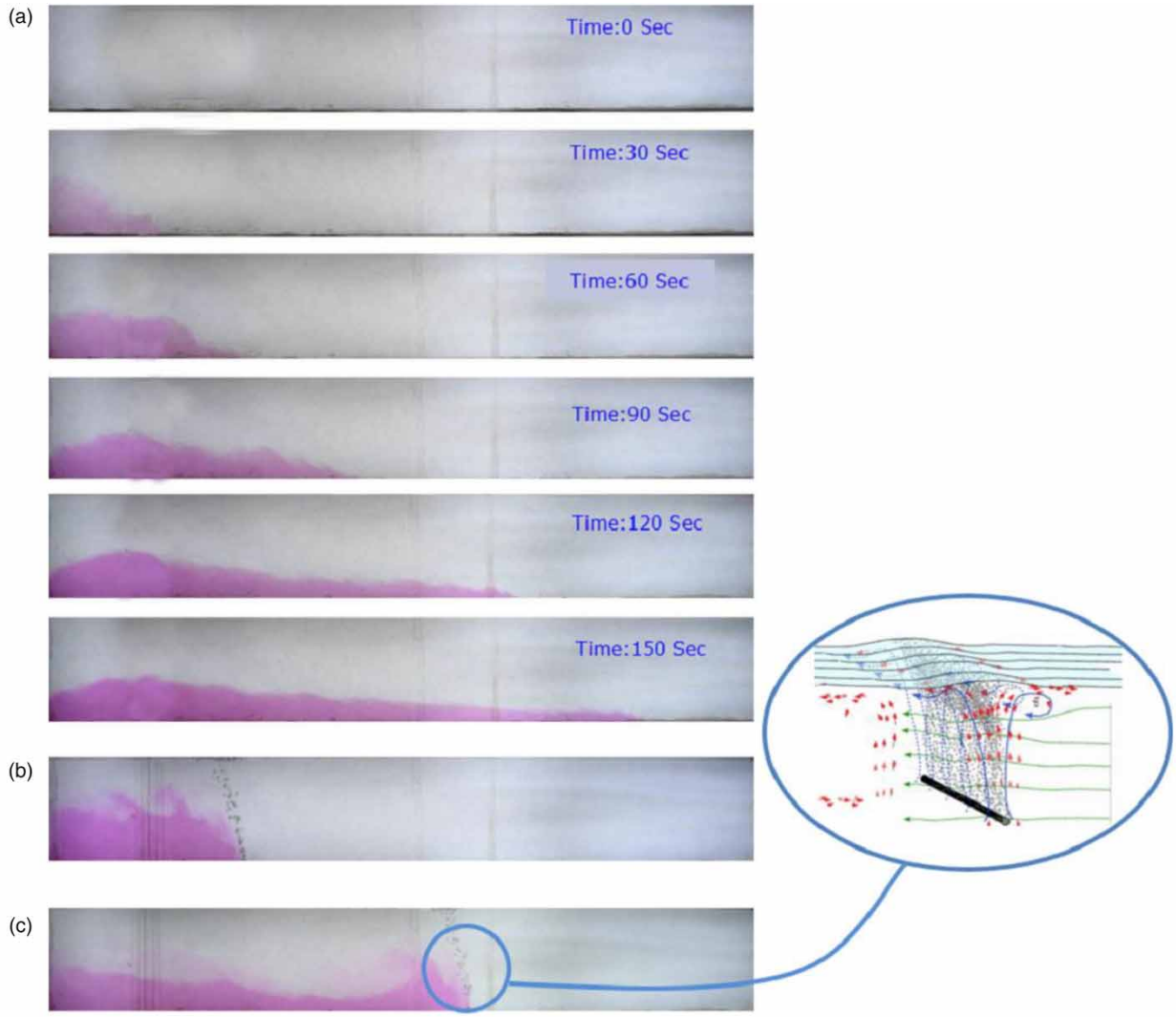

Figure 2 | (a) SWI progress, (b) the first air bubble curtain (Gate I), (c) the second air bubble curtain (Gate II).

that the $V_{frontal}/V_s$ ratio in all cases increases by about 60.6% (average) by a growth in the ρ_s/ρ_f ratio. Also, the effect of ρ_s/ρ_f ratio on the lower range of the Fr number slope of the variation increases shows an active role in the frontal velocity compared with the upper range. In addition, there is an inverse relationship between the Fr number and the $V_{frontal}/V_s$ ratio, i.e., the $V_{frontal}/V_s$ ratio is the highest when the Fr number value is the lowest. The trend of the cases is linear, in the higher range of the Fr number and vice versa. For example, when the Fr number is 0.035 (for cases in which ρ_s/ρ_f ratio is 1.006), the $V_{frontal}/V_s$ ratio is 0.15, while for the cases in which Fr is 0.027, it is 0.34. This indicates about 67% growth for $V_{frontal}/V_s$ ratio when the Fr is decreased by 0.008. For the cases in which ρ_s/ρ_f ratio is 1.010, the changes rate of this value ($V_{frontal}/V_s$ ratio) is about 92%.

The regression equation for the forehead velocity ratio affected by the Froude number and ρ_s/ρ_f is as follows (Equation (7)):

$$\frac{V_{frontal}}{V_s} = 37.61917\frac{\rho_s}{\rho_f} - 24.99835\mathrm{Fr} - 36.82937, \quad R^2 = 0.89 \tag{7}$$

3.2. First ABC equation

Figure 6 indicates the test result for the first ABC, including the effects of Fr_d, Fr, and ρ_s/ρ_f on Q_a/Q_s. Figure 6(a) shows the effect of the Fr_d number on the Q_a/Q_s ratio. The Q_a/Q_s ratio reduces by a rise in Fr_d. The results show that when the Fr_d

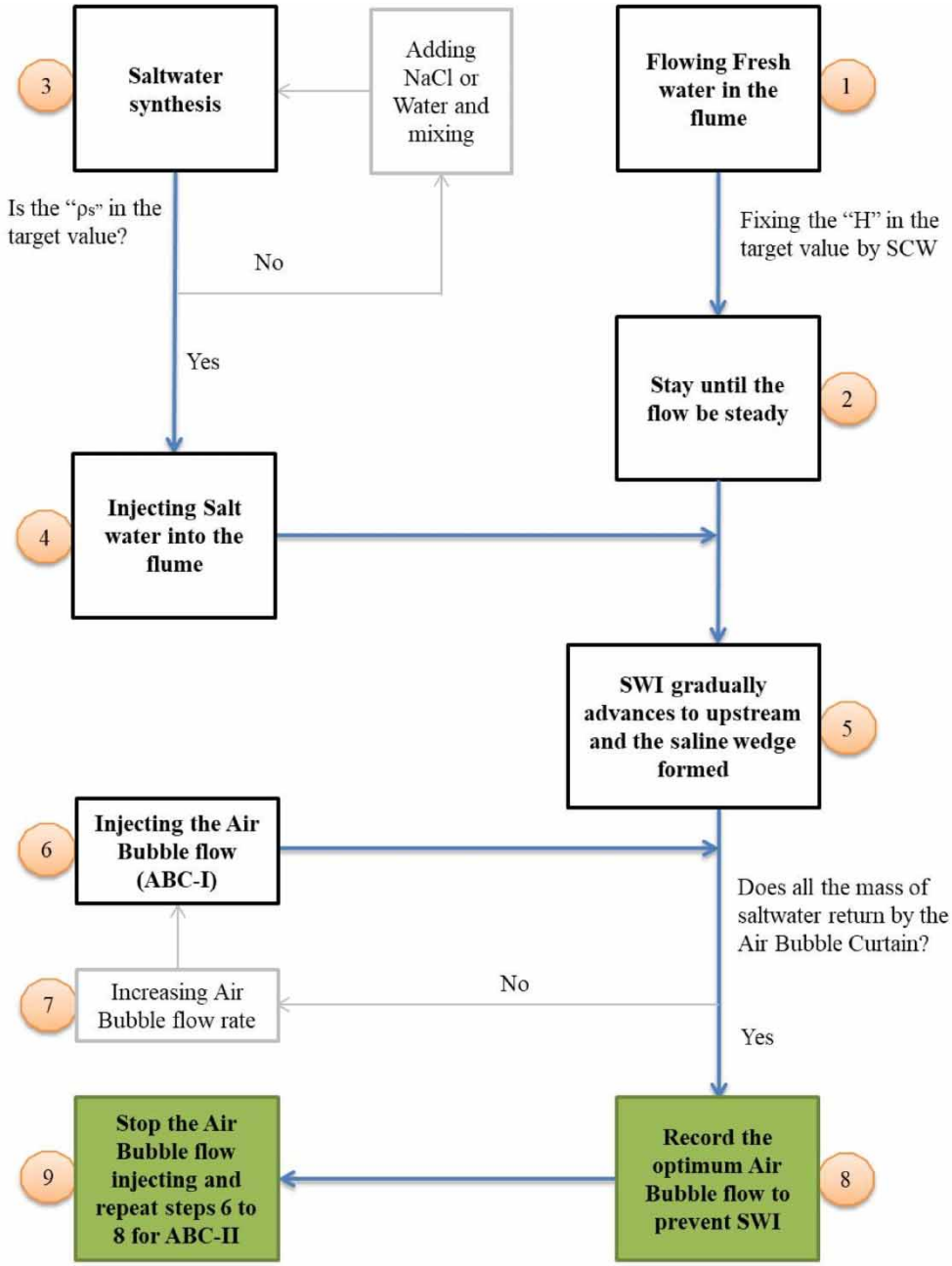

Figure 3 | Flowchart of the research methodology.

number increases by about 65%, the Q_a/Q_s ratio reduces, and this ratio reduces to 59%. When the Fr_d number is low, the Q_a/Q_s ratio is high, and vice versa. Similarly, as reported above, the slope of the changes decreases when the Fr_d number grows. Figure 6(b) demonstrates that the Fr number and ρ_s/ρ_f ratios affect the Q_a/Q_s ratio. When seawater density rises from 1.006 to 1.010, the Q_a/Q_s ratio increases by almost 58% (on average for all cases). Also, the ρ_s/ρ_f ratio grows sharply in the lower ranges of the Fr cases. The graph trend is linear where Fr is higher, and it becomes semi-linear when the Fr is reduced. Also, when the Fr number is 0.035, the Q_a/Q_s ratio is 0.1 (for cases in which ρ_s/ρ_f ratio is 1.006), while for the cases in which Fr is 0.027, it is 0.24. This indicates about 40% growth for Q_a/Q_s ratio when the Fr is decreased by 0.008 units (for cases in which ρ_s/ρ_f ratio is 1.006). Also, this value (Q_a/Q_s ratio) for the cases in which ρ_s/ρ_f ratio is 1.010, the change rate is about 68%.

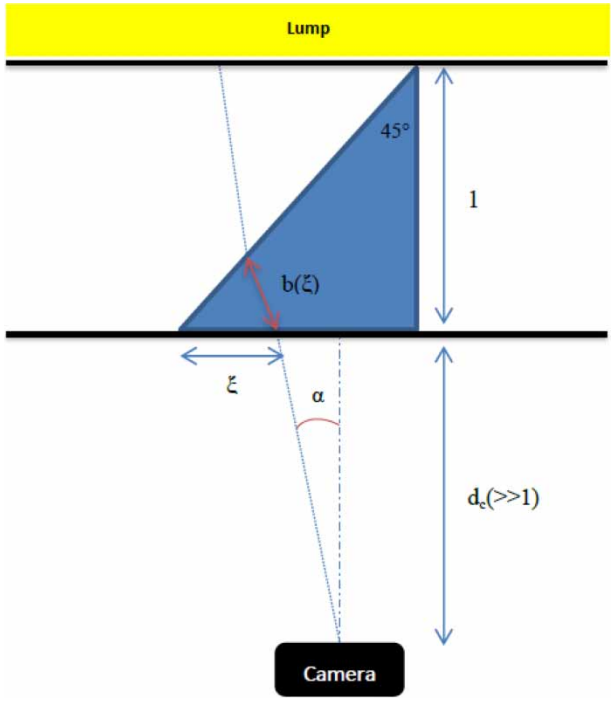

Figure 4 | Plan view of the calibration used to determine the validity of Beer–Lambert Law in the experiments (17).

The regression equation for the first ABC, affected by the Fr number and ρ_s/ρ_f ratio, is presented in the following (Equation (8)):

$$\frac{Q_a}{Q_s} = 30.83333\frac{\rho_s}{\rho_f} - 17.07294\mathrm{Fr} - 30.32099, \quad R^2 = 0.85 \tag{8}$$

3.3. Second ABC equation

Figure 7 indicates the test result for the second ABC, including the effects of $\mathrm{Fr_d}$, Fr, and ρ_s/ρ_f on Q_a/Q_s. As expressed in the previous section, the $\mathrm{Fr_d}$ number has an inverse relationship with the ratio (Q_a/Q_s), which is also true for ABC-II (according to Figure 7(a)). The rate of the Q_a/Q_s is reduced by about 150% when the $\mathrm{Fr_d}$ number is increased by about 65%. The value of the airflow, which is needed to prevent SWI, in the high range of the $\mathrm{Fr_d}$ number significantly, is low. Increasing the Fr number inversely affects the Q_a/Q_s ratio. Contrary to ABC-I, there were multiple behaviours in ABC-II, which can be observed in Figure 7(b). For the Fr numbers greater than 0.03, the ρ_s/ρ_f slope gets close to a constant rate, while for Fr numbers smaller than 0.03, the graph is semi-linear. Also, for the lowest Fr number case, Q_a/Q_s sharply increase. This ratio has increased linearly by rising in the ρ_s/ρ_f ratio. Also, increasing the ρ_s/ρ_f raises the airflow needed to prevent SWI (Q_a/Q_s ratio). When the ρ_s/ρ_f ratio is increased from the lowest to the highest range, the Q_a/Q_s ratio is raised by about 70% (average of all cases). Also, when the Fr number is 0.035, the Q_a/Q_s ratio is 0.07 (for cases in which ρ_s/ρ_f ratio is 1.006), while for the cases in which Fr is 0.027, it is 0.23. This value (Q_a/Q_s ratio) is 0.17 and 0.33 (for the cases in which ρ_s/ρ_f ratio is 1.010), respectively, for the cases where Fr is 0.035 and 0.027.

The regression equation for the second ABC-II, which is affected by Fr number and ρ_s/ρ_f, is as follows (Equation (9)):

$$\frac{Q_a}{Q_s} = 27.33333\frac{\rho_s}{\rho_f} - 15.91913\mathrm{Fr} - 26.85654, \quad R^2 = 0.92 \tag{9}$$

As Figure 8(a) shows, there is shear stress between seawater and freshwater at the interface (boundary layer). The boundary layer is formed, and Kelvin–Helmholtz (KH) is also observed in the boundary layer. As is visible, the mass of the seawater above the green line is returned downstream by the force of the freshwater. At the top of the saline wedge's green line,

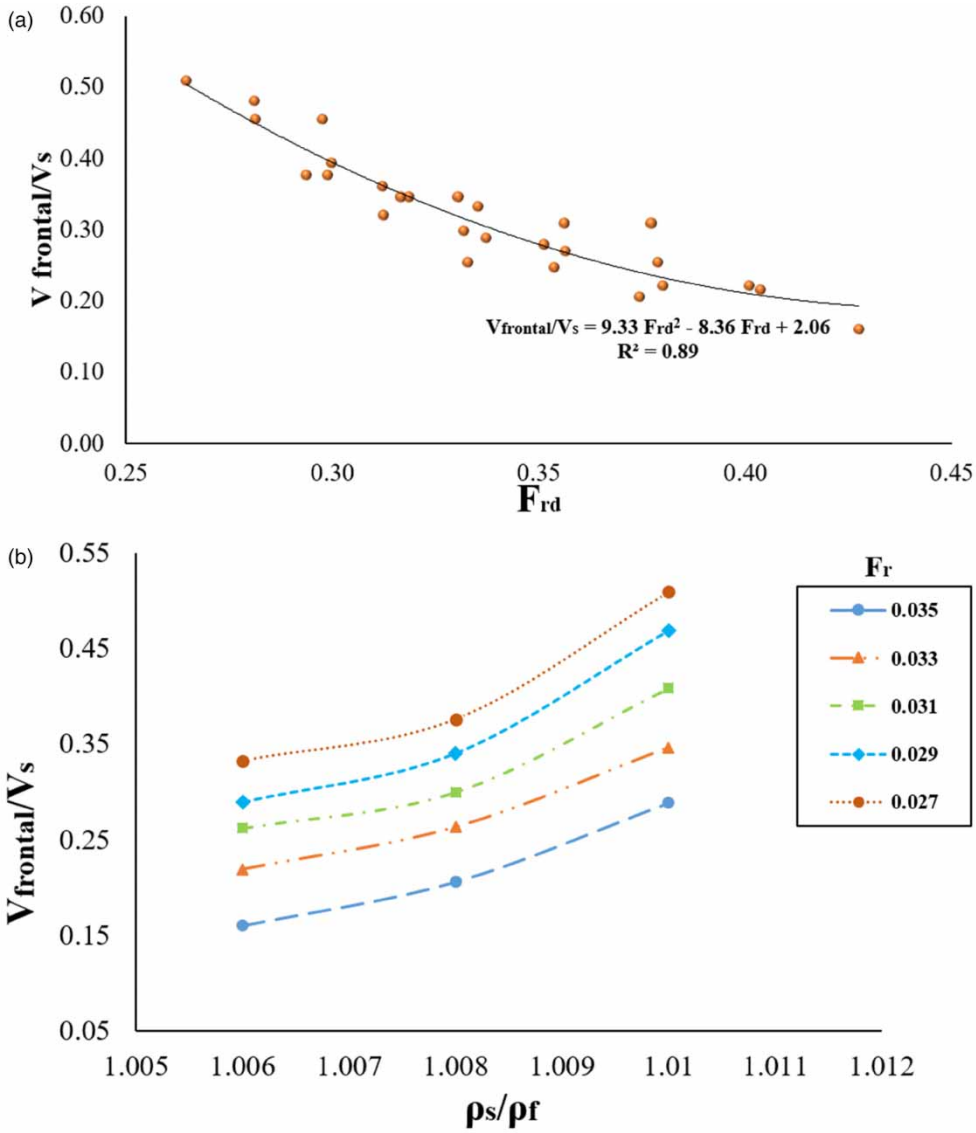

Figure 5 | (a) Ratio of frontal velocity to the Froude number graph; (b) Ratio of frontal velocity to the density ratio graph.

entrainment causes seawater and freshwater to mix. Mixing at the interface helps the density of seawater reduce when it advances upstream. Figure 8(b) illustrates the distribution of seawater concentration along with the saline wedge shown by IPM. It demonstrates that salinity distribution along the channel occurred both horizontally and vertically. As shown in Figure 8(b), the seawater column in the ABC-II is shorter than the ABC-I, and the concentration of seawater in the ABC-II region is lower than ABC-I (about a third of ABC-I).

The prediction chart of V_{frontal}/V_s, Q_a/Q_s for the ABC-I, and Q_a/Q_s for the ABC-II are respectively shown in Figure 8. As shown showed on these graphs, the regression equations are significant to predict the values. Based on Figure 9(b) and 9(c), the prediction of the equation of the ABC-II is more accurate than the ABC-I. The R^2 for ABC-II (Equation (9)) is also higher than ABC-I (Equation (8)).

4. DISCUSSION

The present study explored optimum airflow and suitable location of ABC as a sustainable solution in narrow rivers. Different parameters like seawater density, power of freshwater, power of seawater, and airflow rate directly affect SWI issues. So, analysis of the presented results in the previous section is present in this section.

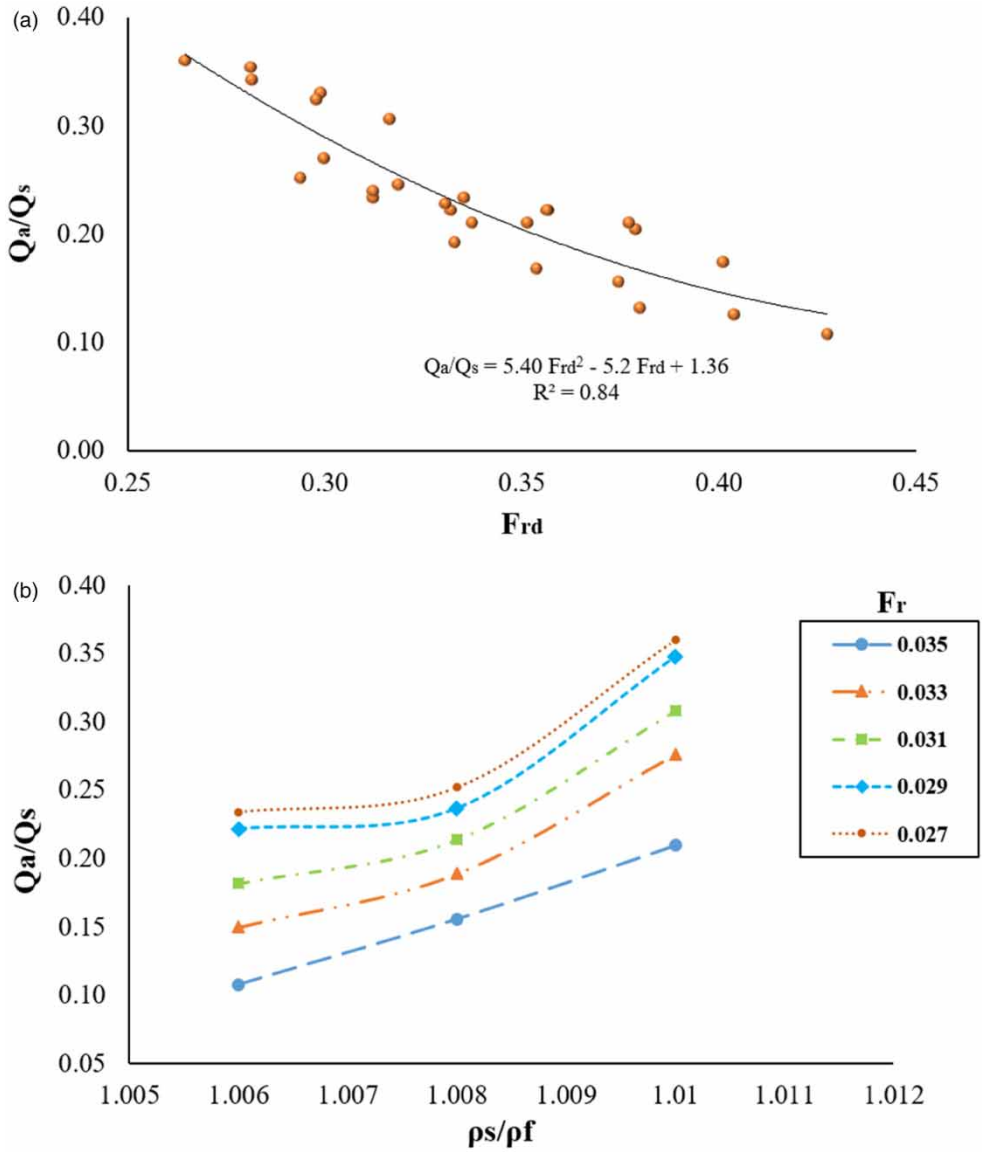

Figure 6 | (a) Ratio of Q_a/Q_s to the densimetric Froude number graph; (b) Ratio of Q_a/Q_s to the density ratio graph in the ABC-I.

The optimum ABC airflow for preventing SWI in different ABC locations depends on the seawater density. As shown in Figures 5(b) and 6(b), the seawater density directly affects the value of airflow for preventing SWI at both ABC-I and ABC-II. As indicated, when the ρ_s/ρ_f ratio increased from 1.006 to 1.010, the $V_{frontal}/V_s$ ratio, Q_a/Q_s for the ABC-I, and Q_a/Q_s for the ABC-II are raised 60, 58, and 70%, respectively. An increase in saline water density leads to more SWI, which was also reported by Talebi & Salehi Neyshabouri (2021). This may be related to an increase in the momentum and convection of the saline water, as a result of which a higher volume of saline water is shaped around the ABC location, requiring more airflow to prevent SWI. Also, the inertia of the saline wedge rises with an increase in seawater density. All the above-mentioned causes some environmental phenomena like KH and Entrainment could not mix the fresh and seawater in their interface (in the higher range of seawater density), so more airflow is required to prevent SWI.

Besides the seawater density, the power of the seawater affects the SWI at the tip of the saline wedge. As reported in Figure 5(b) in the ABC-I, the effect of seawater density in low Fr ranges plays a significant role. This is related to the lack of freshwater power and the high power of seawater. So, both the density and power of the seawater have a direct interaction: seawater power exponentially increases with a rise in seawater density. Contrary to ABC-I, the ABC-II scenario is reverse behaviour. As shown in Figure 6(b), in the greatest Fr cases ($Fr > 0.031$), seawater density changes do not significantly

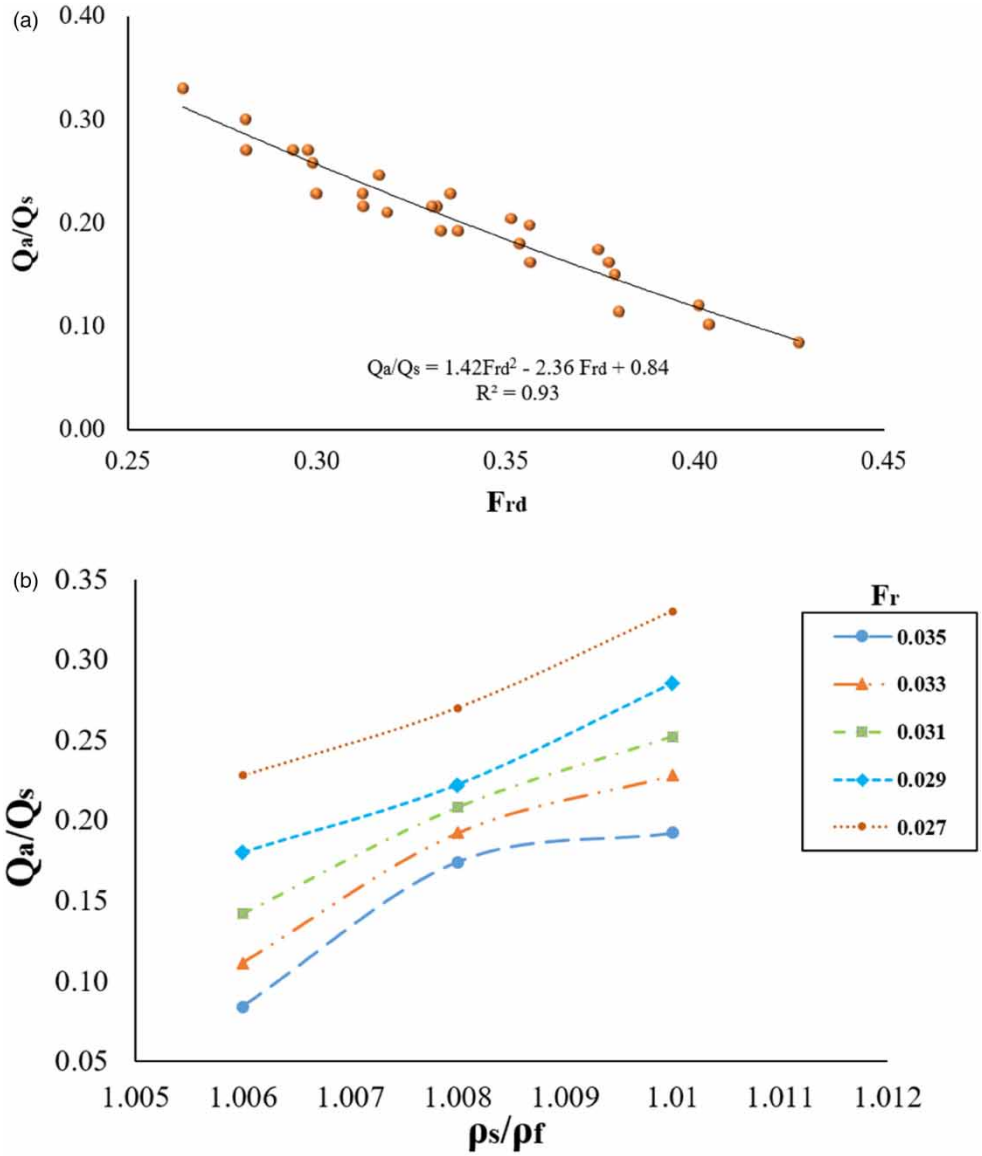

Figure 7 | (a) Ratio of Q_a/Q_s to the densimetric Froude number graph; (b) Ratio of Q_a/Q_s to the density ratio graph in the ABC-II.

affect the process of SWI. It means that a rise in the seawater density does not increase the power of the seawater. The reason for this behaviour is KH in the tip of the saline wedge, which caused seawater to be mixed with freshwater. In other words, the rate of the entrainment and KH are higher than in other regions of the saline wedge. So, an increase in seawater density in the ABC-II does not considerably affect seawater power.

Another factor affecting the optimum ABC airflow value in preventing SWI is the power of freshwater. Mainly, the freshwater power depends on freshwater discharge, velocity, river level, and Fr number. As shown in Figures 5(b) and 6(b), increasing the Fr number in both gates caused the rate of the airflow (Q_a/Q_s) to decrease. As mentioned, when the Fr number changes from 0.035 to 0.027, the $V_{frontal}/V_s$ ratio increases 92%, 67% in cases where ρ_s/ρ_f is 1.010 and 1.006, respectively. These values for the ABC-I raise about 40 and 68%, respectively. Raising the Fr number of the freshwater boosts the freshwater advection; as a result, a higher shear stress rate is exchanged at the interface between the freshwater and seawater. This helps the seawater mass at the boundary layer return downstream by the KH phenomenon and entrainment, which is in line with the finding of Nakai and Arita (2002) and Talebi *et al.* (2022). Also, based on Figure 4(b), increasing in Fr number leads to a decrease in the saline wedge's frontal velocity. Increasing in Fr number accelerates the rate of the KH and entrainment, so the velocity of the saline wedge tip reduces. All the mentioned scenarios indicate that an increase in the freshwater

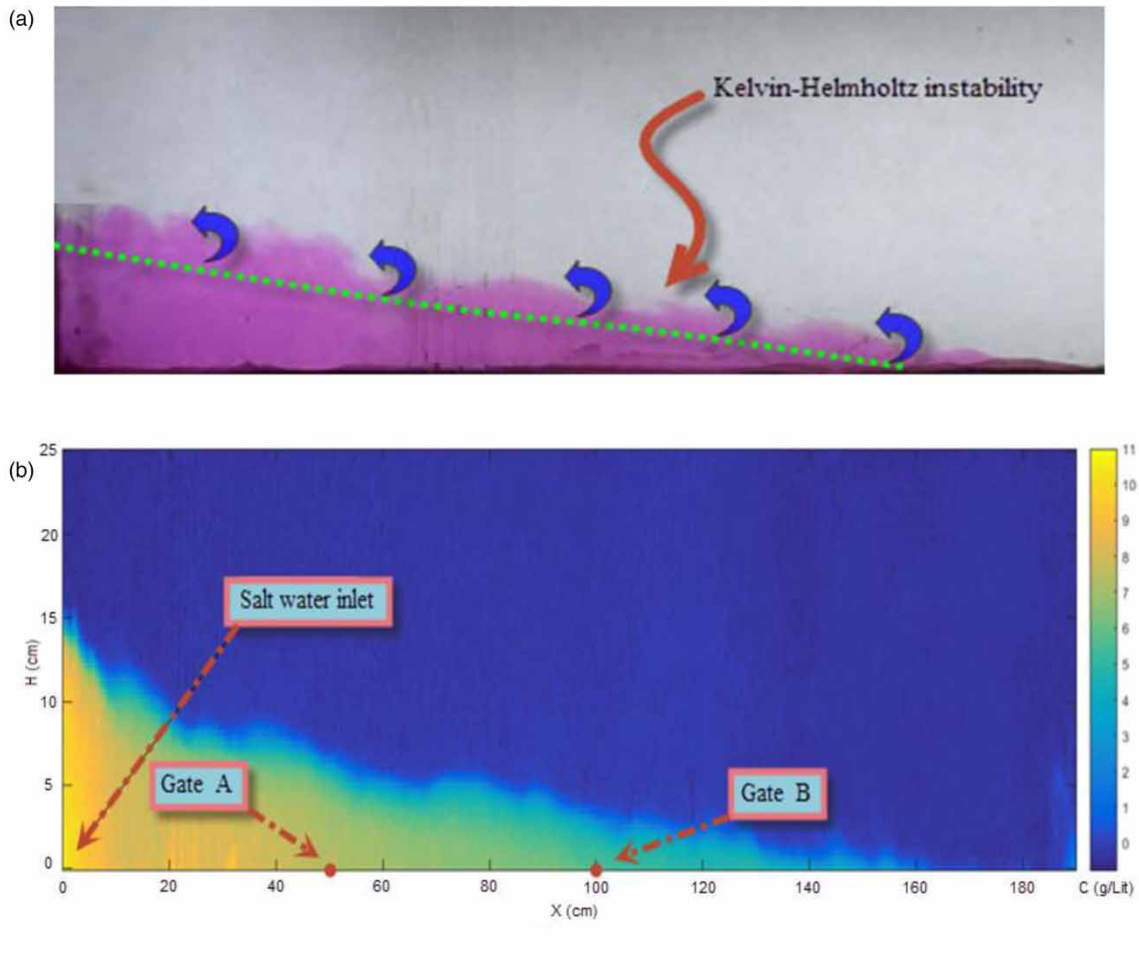

Figure 8 | (a) Boundary layer and KH instability; (b) Distribution graph of saline water concentration along with the saline wedge by IPM. Please refer to the online version of this paper to see this figure in colour: https://dx.doi.org/10.2166/wcc.2023.384.

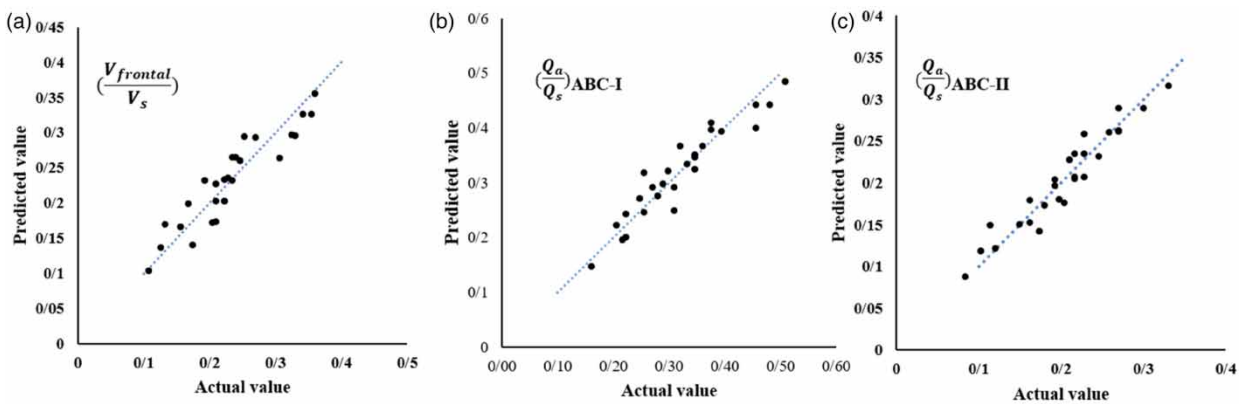

Figure 9 | (a) The predicted value to the actual value chart of $V_{frontal}/V_s$; (b) The predicted value to the actual value of Q_a/Q_s for ABC-I; (c) The predicted value to the actual value chart of Q_a/Q_s in the ABC-II.

power leads to a decrease in the intrusion rate. So, these scenarios subsequently led to less SWI intrusion and less demand for ABC airflow. This is in line with the study by Talebi & Salehi Neyshabouri (2021).

The other important parameter, i.e., determining a suitable location for ABC, depends on some hydrodynamics processes that change the seawater concentration. Based on Figure 7(b), concentration of the saline wedge is decreased when it intrudes

upstream along a river. This means that the seawater movement would balance the seawater gradient due to the exchange between seawater and freshwater. So, it can be clarified that if the ABC is installed in zones near the upstream, less airflow is needed to prevent SWI, while the seawater would pollute more areas of the rivers, and vice versa. Figure 10 presents the performance metrics for the ABC solution for preventing SWI in rivers. According to Figure 10, ABC-1 is a more sustainable solution to prevent SWI because the lowest length of the river is polluted by the seawater, while the height of the seawater on the location of the ABC-1 is higher; consequently cost of running ABC is high. In contrast, the running cost of the ABC in the ABC-II is lower, while the seawater pollutes longer reaches of the river. Also, in the field project, finding a suitable location for the ABC depends on the maximum salinity concentration allowed in a river regarding the consumption (drinking, agriculture, factory, etc.). So, a good location for installing ABC in any field project is different, and the mentioned factors must be considered in the design of an ABC project to be cost-effective.

In summary, the optimum location of the ABC and optimum value of the airflow to control the SWI is affected by some parameters like seawater density, power of the freshwater, and power of the seawater, which are studied in this section.

5. SUMMARY AND CONCLUSION

Many countries worldwide have been endangered because of SLR and climate change in recent years. SWI, as a result of SLR and climate change, can damage freshwater resources along rivers. Developing a sustainable solution to alleviate this concern has attracted a lot of attention. In the same line, the present study explored optimum airflow and suitable location of ABC as a sustainable solution in narrow rivers.

In conclusion, the present study investigated the effect of ABC location and airflow demand on SWI. To this end, several experimental tests were performed by assuming different values for the river and airflow discharges as well as for the salinity.

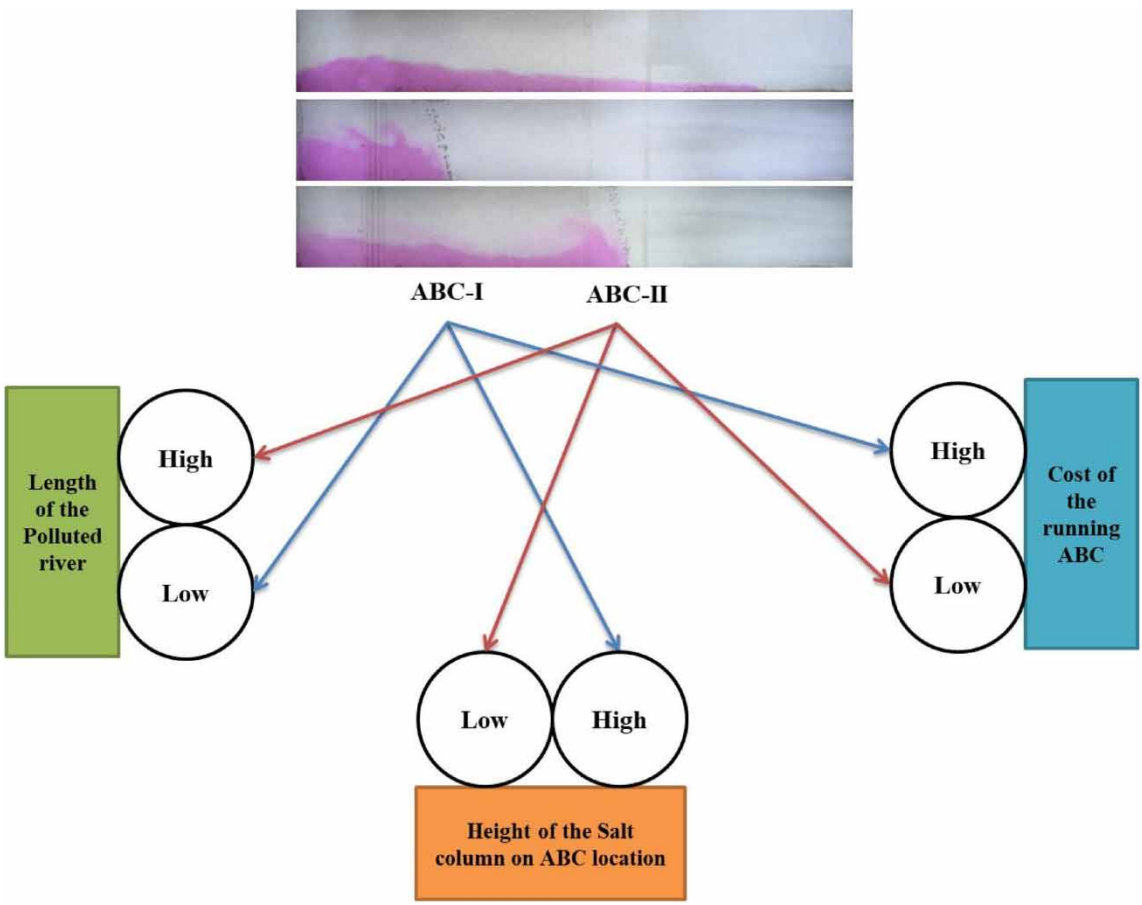

Figure 10 | Performance metrics of air bubble curtain.

In addition, two ABCs were located near and far from the downstream. The results showed that the optimal value of the air bubbles required to control SWI depends mostly on the density of seawater, with more airflow required to control denser flows. In other words, when the ρ_s/ρ_f ratio increased from 1.006 to 1.010, the $V_{frontal}/V_s$ ratio, Q_a/Q_s for the ABC-I, and Q_a/Q_s for the ABC-II are raised by 60, 58, and 70%, respectively. Also, when the Fr $>$ 0.031, seawater density changes do not significantly affect the process of SWI.

Another important parameter is the freshwater discharge and its corresponding Froude number. In the experiments, Fr numbers were chosen based on a low velocity of freshwater under estuaries and laboratory limitations. Results indicate that when the Fr number changes from 0.035 to 0.027, the $V_{frontal}/V_s$ ratio increases by 92 and 67% in cases where ρ_s/ρ_f is 1.010 and 1.006, respectively. These values for the ABC-I raise about 40 and 68%, respectively. The results show that as the Froude number of freshwater increases, the SWI value and the airflow required to control it decrease. In addition, the ABC closer to the river downstream requires higher airflow rates to completely control the SWI and decrease the pollution extension.

Eventually, the regression equations for predicting the SWI parameters were derived based on the flow properties. Clearly, the equations have been derived based on some general assumptions and laboratory limitations, for example, flume geometry, Froude number, etc., yet they can be utilized efficiently for the initial design and for predicting the required range of the airflow and approximate location of the ABCs to control unwanted SWI properly. It goes without saying that the exact design of the optimal point in a real case and its corresponding airflow parameters depend on local conditions such as river geometry, water quality, financial costs for ABC construction, environmental issues, etc. This system may only be applicable to narrow rivers in some specific ranges.

Finally, this study has some limitations. All the tests studied the SWI in a limited density range of the sweater. At the same time, the seawater concentration in an actual condition is sometimes four times greater than the studied density. For this study, NaCl is considered for seawater synthesis, while natural seawater may have different properties in the field. Also, experiments were conducted in a specific range of the Fr number of freshwater. In addition, some physical assumption considered in this investigation includes: (1) the slope of the flume is zero, (2) the cross-section is rectangular, (3) there is no friction between the flume and water, (4) the injected air pressure is 1 atm, and (5) the water temperature is around 25 °C. Future studies are recommended to investigate other unknown parameters, including the effects of vegetation as a natural barrier against SWI prevention. Besides, investigation on the cross variation of airflow and its effect on SWI patterns can be interesting due to the unbalanced seawater and river velocity profile distribution.

ACKNOWLEDGEMENT

This study was supported by the Tarbiat Modares University, Tehran, Iran.

DATA AVAILABILITY STATEMENT

All relevant data are included in the paper or its Supplementary Information.

CONFLICT OF INTEREST

The authors declare there is no conflict.

REFERENCES

Abd-Elhamid, H., Javadi, A., Abd-Elaty, I. & Sherif, M. 2016 Simulation of seawater intrusion in the Nile Delta aquifer under the conditions of climate change. *Hydrology Research* **47** (6), 1198–1210. https://doi.org/10.2166/nh.2016.157.

Abd-Elhamid, H., Abdelaty, I. & Sherif, M. 2019 Evaluation of potential impact of Grand Ethiopian Renaissance Dam on seawater intrusion in the Nile Delta aquifer. *International Journal of Environmental Science and Technology.* **16** (5), 2321–2332.

Asaeda, T., Arita, M. & Pham, H. D. 1997 Prevention of saline wedge intrusion by an air curtain in an estuary. *Doboku Gakkai Ronbunshu* **572**, 23–31. https://doi.org/10.2208/jscej.1997.572_23.

Bacot, A., Frank, D. & Linden, P. F. 2022 Bubble curtains used as barriers across horizontal density stratifications. *Journal of Fluid Mechanics* **941**. https://doi.org/10.1017/jfm.2022.142.

Barlow, P. M. & Reichard, E. G. 2010 Saltwater intrusion in coastal regions of North America. *Hydrogeology Journal* **18** (1), 247–260. https://doi.org/10.1007/s10040-009-0514-3.

Bhagat, C., Khandekar, A., Singh, A. & Mohapatra, K. 2021 Delineation of submarine groundwater discharge and seawater intrusion zones using anomalies in the field water quality parameters, groundwater level fluctuation and sea surface temperature along the Gujarat coast of India. *Journal of Environmental Management* **296**. https://doi.org/10.1016/j.jenvman.2021.113176.

Burgan, H. I., Vaheddoost, B. & Aksoy, H. 2017 Frequency analysis of monthly runoff in intermittent rivers. In *World Environmental & Water Resources Congress (EWRI 2017)*, 21–25 May 2017, Sacramento, CA, USA, pp. 327–334. https://doi.org/10.1061/9780784480625.030.

Chebana, F. & Ouarda, T. B. 2021 Multivariate non-stationary hydrological frequency analysis. *Journal of Hydrology* **593**, 125907. https://doi.org/10.1016/j.jhydrol.2020.125907.

Chun, J., Lim, C., Kim, D. & Kim, J. 2018 Assessing impacts of climate change and sea-level rise on seawater intrusion in a coastal aquifer. *Water* **10** (4), 357.

Ekeleme, A. C., Ekwueme, B. N. & Agunwamba, J. C. 2021 Modeling contaminant transport of nitrate in soil column. *Emerging Science Journal*. http://dx.doi.org/10.28991/esj-2021-01290

Erostate, M., Huneau, F., Garel, E., Ghiotti, S., Vystavna, Y., Garrido, M. & Pasqualini, V. 2020 Groundwater dependent ecosystems in coastal Mediterranean regions: characterization, challenges and management for their protection. *Water Research* **172**, 115461.

Ghisalberti, M. & Nepf, H. 2005 Mass transport in vegetated shear flows. *Environmental Fluid Mechanics* **5**, 527–551.

Han, D. & Currell, M. J. 2018 Delineating multiple salinization processes in a coastal plain aquifer, Northern China: hydrochemical and isotopic evidence. *Hydrology and Earth System Sciences* **22** (6), 3473–3491. https://doi.org/10.5194/hess-22-3473-2018.

Karamouz, M., Zeynolabedin, A. & Olyaei, M. A. 2016 Regional drought resiliency and vulnerability. *Journal of Hydrologic Engineering* **21** (11), 05016028.

Larsen, S. J., Kilminster, K. L., Mantovanelli, A., Goss, Z. J., Evans, G. C., Bryant, L. D. & McGinnis, D. F. 2019 Artificially oxygenating the Swan River estuary increases dissolved oxygen concentrations in the water and at the sediment interface. *Ecological Engineering* **128**, 112–121. https://doi.org/10.1016/j.ecoleng.2018.12.032.

Llopis-Albert, C. & Pulido-Velazquez, D. 2015 Using MODFLOW code to approach transient hydraulic head with a sharp-interface solution. *Hydrological Processes* **29** (8), 2052–2064.

Nakai, M. & Arita, M. 2002 An experimental study on prevention of saline wedge intrusion by an air curtain in rivers. *Journal of Hydraulic Research* **40**, 333–339. https://doi.org/10.1080/00221680209499947.

Nazarnia, H., Nazarnia, M., Sarmasti, H. & Wills, W. O. 2020 A systematic review of civil and environmental infrastructures for coastal adaptation to sea level rise. *Civil Engineering Journal*. http://dx.doi.org/10.28991/cej-2020-03091555.

Oldeman, A. M., Kamath, S., Masterov, M. V., O'Mahoney, T. S. D., Van-Heijst, G. J. F., Kuipersa, J. A. M. & Buista, K. A. 2020 Numerical study of bubble screens for mitigating salt intrusion in sea locks. *International Journal of Multiphase Flow* **129**, 103321. https://doi.org/10.1016/j.ijmultiphaseflow.2020.103321.

Palacios, A., Ledo, J. J., Linde, N., Luquot, L., Bellmunt, F., Folch, A., Marcuello, A., Queralt, P., Pezard, P. A., Martínez, L., Val, L. D., Bosch, D. & Carrera, J. 2020 Time-lapse cross-hole electrical resistivity tomography (CHERT) for monitoring seawater intrusion dynamics in a Mediterranean aquifer. *Hydrology and Earth System Sciences* **24** (4), 2121–2139. https://doi.org/10.5194/hess-24-2121-2020.

Panpan, L., Jian, S., Jianfeng, W. & Jichun, W. 2021 A numerical simulation study for controlling seawater intrusion by using hydraulic and physical barriers. *Hydrogeology & Engineering Geology* **48** (4), 32–40. doi: 10.16030/j.cnki.issn.1000-3665.202007068.

Sasaki, T. & Asaeda, T. 1993 Air curtain for preventing the salt water intrusion in estuaries. *Environmental Systems Research* **21**, 335–339. https://doi.org/10.2208/proer1988.21.335.

Talebi, A. & Salehi Neyshabouri, S. A. A. 2021 Effect of freshwater river level, seawater density and efficiency of air bubble curtain system on preventing saline water intrusion in surface water. *Sharif J Civ Eng.* https://dx.doi.org/10.24200/j30.2020.55273.2717.

Talebi, A., Salehi Neyshabouri, S. A. A. & Khoshgou, H. 2022 Investigation on factors affecting the performance of the air bubble curtain in preventing the penetration of salinity. *International Journal of Environmental Science and Technology* 1–14.

Torres-Martinez, J. A., Mora, A., Ramos-Leal, J. A., Morán-Ramírez, J., Arango-Galván, C. & Mahlknecht, J. 2019 Constraining a density-dependent flow model with the transient electromagnetic method in a coastal aquifer in Mexico to assess seawater intrusion. *Hydrogeology Journal* **27** (8), 2955–2972.

van der Ven, P., O'Mahoney, T. S. & Weiler, O. 2018 *Methods to Assess Bubble Screens Applied to Mitigate Salt Intrusion Through Locks*. PIANC-World Congress Panama City, Panama City, pp. 1–17.

Zeynolabedin, A. & Ghiassi, R. 2019 The SIVI index: a comprehensive approach for investigating seawater intrusion vulnerability for island and coastal aquifers. *Environmental Earth Sciences* **78** (24), 1–10.

Yusuf, H., Azis, A. & Badaruddin, S. 2022 Physical modeling of sand columns application in recharge reservoir to prevent seawater intrusion. *Water Science & Technology Water Supply* **22**(6). DOI:10.2166/ws.2021.365.

Zeynolabedin, A., Ghiassi, R. & Dolatshahi Pirooz, M. 2021a Seawater intrusion vulnerability evaluation and prediction: a case study of Qeshm Island, Iran. *Journal of Water and Climate Change* **12** (1), 265–277.

Zeynolabedin, A., Ghiassi, R., Norooz, R., Najib, S. & Fadili, A. 2021b Evaluation of geoelectrical models efficiency for coastal seawater intrusion by applying uncertainty analysis. *Journal of Hydrology* **603**, 127086.

Zhang, Z. & Savenije, H. 2019 Maximum power of saline and fresh water mixing in estuaries. *Earth System Dynamics* **10** (4), 667–684. https://doi.org/10.5194/esd-10-667-2019.

Zheng, H., Wenxi, L., Yue, F., Tiansheng, M., Jin, L. & Jiuhui, L. 2021 Optimal location of cutoff walls for seawater intrusion. *Applied Water Science* **11**, 179. https://doi.org/10.1007/s13201-021-01514-1.

First received 8 September 2022; accepted in revised form 25 December 2022. Available online 12 January 2023